sustainability

MDPI

Article

Integrating UAV LiDAR and Multispectral Data for Aboveground Biomass Estimation in High-Andean Pastures of Northeastern Peru

Angel J. Medina-Medina [1], Samuel Pizarro [1], Katerin M. Tuesta-Trauco [1], Jhon A. Zabaleta-Santisteban [1], Abner S. Rivera-Fernandez [1], Jhonsy O. Silva-López [2], Rolando Salas López [1], Renzo E. Terrones Murga [3], José A. Sánchez-Vega [1], Teodoro B. Silva-Melendez [1], Manuel Oliva-Cruz [1], Elgar Barboza [1] and Alexander Cotrina-Sanchez [1,*]

[1] Instituto de Investigación para el Desarrollo Sustentable de Ceja de Selva (INDES-CES), Universidad Nacional Toribio Rodríguez de Mendoza de Amazonas, Chachapoyas 01001, Peru; angel.medina@untrm.edu.pe (A.J.M.-M.); samuel.pizarro@untrm.edu.pe (S.P.); katerin.tuesta.epg@untrm.edu.pe (K.M.T.-T.); jhon.zabaleta.epg@untrm.edu.pe (J.A.Z.-S.); abner.rivera.epg@untrm.edu.pe (A.S.R.-F.); rolando.salas@untrm.edu.pe (R.S.L.); ander.jasv18@gmail.com (J.A.S.-V.); 7680096361@untrm.edu.pe (T.B.S.-M.); manuel.oliva@untrm.edu.pe (M.O.-C.); elgar.barboza@untrm.edu.pe (E.B.)

[2] Área de Cartografía y Teledetección, Laboratorio de Agrostología, Instituto de Investigación en Ganadería y Biotecnología, Facultad de Ingeniería Zootecnista, Agronegocios y Biotecnología, Universidad Nacional Toribio Rodríguez de Mendoza de Amazonas, Chachapoyas 01001, Peru; jhonsy.silva@untrm.edu.pe

[3] Lidar Peru Sociedad Cerrada, Av. Alfredo Benavides Nro. 1944, Lima 15047, Peru; renzo@lidar.pe

* Correspondence: alexander.cotrina@untrm.edu.pe

Abstract

Accurate estimation of aboveground biomass (AGB) is essential for monitoring forage availability and guiding sustainable management in high-altitude pastures, where grazing sustains livelihoods but also drives ecological degradation. Although remote sensing has advanced biomass modeling in rangelands, applications in Andean–Amazonian ecosystems remain limited, particularly using UAV-based structural and spectral data. This study evaluated the potential of UAV LiDAR and multispectral imagery to estimate fresh and dry AGB in ryegrass (*Lolium multiflorum* Lam.) pastures of Amazonas, Peru. Field data were collected from subplots within 13 plots across two sites (Atuen and Molinopampa) and modeled using Random Forest (RF), Support Vector Machines, and Elastic Net. AGB maps were generated at 0.2 m and 1 m resolutions. Results revealed clear site- and month-specific contrasts, with Atuen yielding higher AGB than Molinopampa, linked to differences in climate, topography, and grazing intensity. RF achieved the best accuracy, with chlorophyll-sensitive indices dominating fresh biomass estimation, while LiDAR-derived height metrics contributed more to dry biomass prediction. Predicted maps captured grazing-induced heterogeneity at fine scales, while aggregated products retained broader gradients. Overall, this study shows the feasibility of UAV-based multi-sensor integration for biomass monitoring and supports adaptive grazing strategies for sustainable management in Andean–Amazonian ecosystems.

Keywords: Chachapoyas pastures; pasture productivity; highland ecosystems; rotational grazing; UAV remote sensing

check for updates

Academic Editor: Chao Gai

Received: 24 September 2025
Revised: 26 October 2025
Accepted: 30 October 2025
Published: 31 October 2025

Citation: Medina-Medina, A.J.; Pizarro, S.; Tuesta-Trauco, K.M.; Zabaleta-Santisteban, J.A.; Rivera-Fernandez, A.S.; Silva-López, J.O.; Salas López, R.; Terrones Murga, R.E.; Sánchez-Vega, J.A.; Silva-Melendez, T.B.; et al. Integrating UAV LiDAR and Multispectral Data for Aboveground Biomass Estimation in High-Andean Pastures of Northeastern Peru. *Sustainability* **2025**, *17*, 9745. https://doi.org/10.3390/su17219745

Copyright: © 2025 by the authors. Licensee MDPI, Basel, Switzerland. This article is an open access article distributed under the terms and conditions of the Creative Commons Attribution (CC BY) license (https://creativecommons.org/licenses/by/4.0/).

1. Introduction

Grasslands are among the most extensive and dominant terrestrial biomes, covering approximately 52.5 million km^2, which represents around 40% of the Earth's land surface [1,2]. These ecosystems play a crucial role as carbon sinks, contribute to erosion control, provide forage for livestock, and support rural communities that depend directly on their productivity [3–5]. In Peru, by 2012, natural pastures covered 18.97 million hectares (14.76% of the national territory), and this area has continued to expand in Amazonian regions, mainly through monocultures, and in high-Andean regions through programs promoting pasture establishment in rural livestock zones [6,7]. Beyond providing forage for domestic animals such as cattle, sheep, and South American camelids, high-Andean pastures have been shown to act as reservoirs of soil organic carbon [8,9]. However, these ecosystems are increasingly threatened by land-use change, fires, overgrazing, and inadequate management practices [10,11]. Such pressures reduce forage productivity, alter soil structure and fertility, limit hydrological regulation, and compromise key ecosystem services essential for livestock sustainability and ecosystem resilience in the Andes [12,13].

Given this context, accurate and scalable estimation of aboveground biomass (AGB) is essential to assess the productive capacity of grasslands, guide restoration planning, and support grazing management [14,15]. Traditional methods of AGB estimation at local scales—whether visual or destructive approaches such as clipping, drying, and weighing vegetation—are accurate but costly, labor-intensive, and impractical for extensive or high-frequency monitoring [16–18]. Likewise, non-destructive and low-cost field methods, such as the disk pasture meter, pin-frame or point-intercept, and Robel pole visual obstruction, require site-specific calibration, are time-consuming, and have limitations in heterogeneous or large-scale environments [19–21].

Remote sensing offers an efficient, non-destructive alternative for AGB estimation at different spatial scales, enabling data acquisition at lower cost and shorter time intervals, and facilitating extensive monitoring [22,23]. AGB estimation has been explored using radar data from Sentinel-1 [24], and temporal dynamics derived from vegetation indices (VIs) obtained from passive sensors such as MODIS, Sentinel-2, Landsat, or combinations thereof [25–27]. In particular, MODIS-derived NDVI has enabled AGB estimation in Andean ecosystems of Peru and Colombia; however, validation with spectrometry or in situ sampling is needed for more accurate predictions [28,29]. Furthermore, the orographic effect of the Andes results in high cloud cover across eastern slopes and páramos for much of the year, limiting the continuous acquisition of optical data [30,31]. This highlights the need to explore unmanned aerial platforms, such as unmanned aerial vehicles (UAVs), which offer high-resolution spatial and temporally flexible data acquisition.

UAVs, with their flexible spatial and temporal resolution, are highly effective tools for monitoring AGB in pastures and forage systems, providing critical insights for livestock management [32]. Equipped with multispectral cameras, UAVs enable the derivation of vegetation indices, with NDVI being the most widely applied [33]. Low-cost RGB imagery has also proven effective in predicting AGB, particularly when combined with additional VIs [34] and machine learning techniques such as Random Forest (RF) [35] or other modeling approaches [36]. AGB estimation accuracy can be improved by integrating structural metrics, such as canopy height models (CHM), across different pasture growth stages [37]. These metrics can be derived from LiDAR data acquired via UAVs or terrestrial laser scanning (TLS), as demonstrated in Belgium [38] and applied to rotational grazing systems in Germany, contributing to precision livestock management [39]. Although multispectral UAVs have been used to estimate AGB in high-Andean grasslands of Ecuador [15] and Colombia [36], such studies remain scarce in Peru, with a few specific cases in crops such as oats (*Avena sativa* L.) in the central highlands [40].

Therefore, this study aims to develop and validate a methodology to estimate AGB, both fresh and dry, in *L. multiflorum* (ryegrass) pastures within high-Andean silvopastoral systems in Amazonas, Peru. Specifically, the study (i) integrates UAV-based LiDAR structural metrics and multispectral indices with field measurements of fresh and dry biomass, and (ii) applies and evaluates machine learning algorithms to predict AGB and assess model accuracy at fine spatial scales. By linking fine-scale remote sensing with ground data, this research seeks to establish a methodological basis for monitoring grassland productivity, supporting sustainable management of extensive grazing and soil conservation in Andean–Amazonian ecosystems.

2. Materials and Methods

2.1. Study Area

The study areas were located in livestock basins encompassing the districts of Leimebamba (or Leymebamba) and Molinopampa, in the Amazonas region of Peru, where extensive cattle ranching and the presence of *L. multiflorum* (ryegrass) pastures predominate, forming part of high-Andean silvopastoral systems with mixed native and introduced grass species [41,42]. Atuen, located in Leimebamba, lies in a valley with gentle slopes and relatively uniform pasture cover, whereas Molinopampa features steeper terrain, fragmented grasslands, and more intensive rotational grazing managed through a combination of electric and live fencing. These contrasting conditions represent the typical topographic and management variability of Andean pastures in northeastern Peru, where livestock production remains a key activity and silvopastoral systems are increasingly promoted as sustainable alternatives for pasture management under humid montane conditions in the Peruvian Amazon [7]. The Leimebamba and Molinopampa zones range in altitude from 2300 to 3200 m a.l.s., with mean annual temperatures between 6.4 °C and 27.1 °C, and annual precipitation ranging from 382 to 2708 mm. The climate is humid temperate, with a rainy period from November to April and a drier season from May to October, showing precipitation peaks between January and March [43]. Soils that are rich in organic matter with near-neutral pH provide optimal conditions for pasture development, although they are susceptible to degradation under prolonged overgrazing practices [13].

The study was conducted in the sectors of Atuen (Lat. 6°53′14″ S, 77°46′39″ W) and Molinopampa (Lat. 6°12′42″ S, 77°40′38″ W), both located in the province of Chachapoyas, Amazonas, Peru (Figure 1a). Initially, a total of 60 plots (30 plots of 30 × 30 m per site) were established across both sectors. From these, seven plots in Molinopampa (Figure 1b), and six plots in Atuen (Figure 1c) were selected for field data collection. The selection focused on plots with homogeneous topography and pasture cover, while avoiding natural or anthropogenic barriers such as small streams, rocky outcrops, and live fences. This latter factor was particularly considered in Molinopampa to ensure UAV flight safety and to minimize potential interference from leaf litter or shading produced by bordering trees. Additionally, considering that both sites are managed under extensive rotational grazing, the arrangement of electric fences controlling grazing rotation was also taken into account to minimize livestock interference during field data collection. Within each selected plot, five 1 × 1 m subplots were established for aboveground biomass sampling (Figure 1d,e).

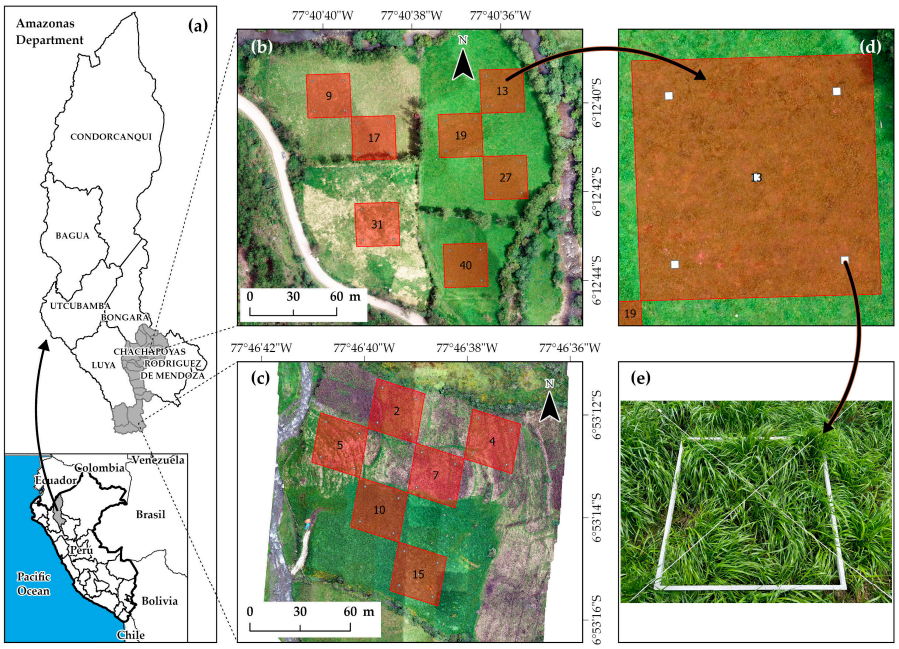

Figure 1. Study areas in Chachapoyas Province, Amazonas, Peru: (**a**) overall location; (**b**) Molinopampa with seven selected plots; (**c**) Atuen with six selected plots; (**d**) example of a subplot with five sampling frames; (**e**) 1 × 1 m frame used for biomass collection. Numbers in (**b**,**c**) indicate individual plot codes.

2.2. Methodological Framework

The workflow shown in Figure 2 illustrates the three main stages of this study: (a) acquisition of multispectral imagery using UAVs, from which orthomosaics were generated and VIs were calculated; (b) LiDAR surveys with the same UAV to obtain structural metrics, such as the CHM and attributes derived from the point cloud; and (c) field collection of fresh biomass data in sampling plots. All this information was integrated to train and validate machine learning models aimed at the non-destructive estimation and monitoring of AGB in high-Andean pastures.

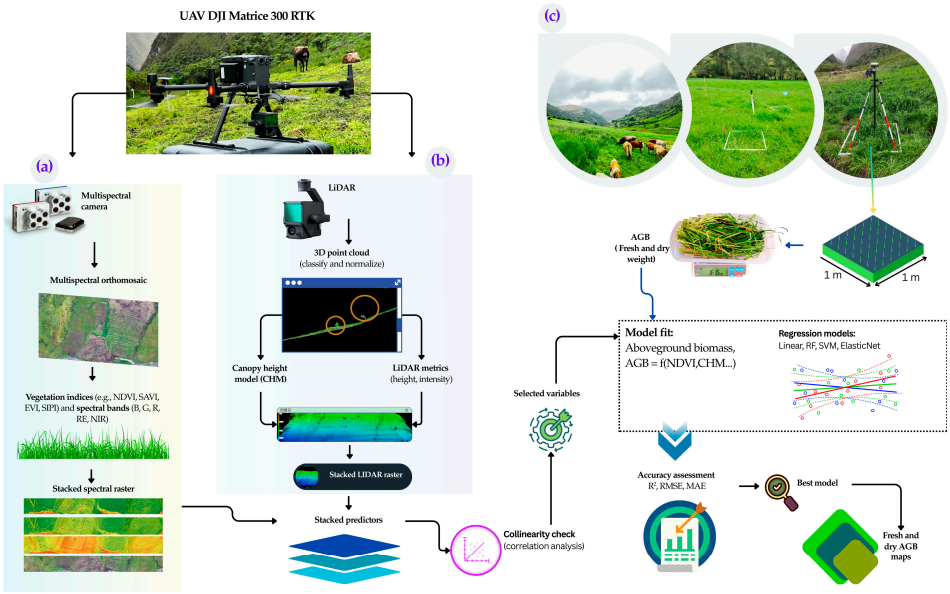

Figure 2. Workflow for estimating aboveground biomass (AGB) in high-altitude Andean pastures using UAVs, combining (**a**) multispectral imagery, (**b**) LiDAR data, and (**c**) field measurements, processed using machine learning models.

2.3. UAV Data Acquisition and Processing

A DJI Matrice 300 RTK UAV was used to conduct two flights per site, scheduled to coincide with the livestock rotation cycle and pasture regrowth. In the Atuen sector, flights were carried out on 10 February and 10 March 2025, while in the Molinopampa sector, they took place on 27 March and 27 April 2025. For each flight, ground control points (GCPs) were established and measured using Global Navigation Satellite System (GNSS) receivers with real-time kinematic (RTK) correction, achieving centimeter-level accuracy.

2.3.1. Multispectral Data

A MicaSense RedEdge-MX multispectral camera, mounted on the UAV was employed to capture imagery across ten spectral bands: Blue (475 ± 32 nm), Green (560 ± 27 nm), Red (668 ± 14 nm), Red Edge (717 ± 12 nm), NIR (840 ± 40 nm), Coastal Blue (444 ± 28 nm), Green2 (531 ± 14 nm), Red2 (650 ± 16 nm), RedEdge2 (705 ± 10 nm), and RedEdge3 (740 ± 18 nm) [44]. Flight parameters were optimized to ensure both spectral integrity and spatial consistency: altitude of 40 m, flight speed of 4 m s^{-1}, capture interval of 1 s, overlap >75%, and storage in 16-bit TIFF format. Data were acquired between 11:00 and 13:00 under clear or fully overcast conditions to minimize shadow effects, given the highly unpredictable weather and frequent cloud cover typical of Andean ecosystems [45].

For multispectral image processing, Pix4D Mapper software (version 4.1) was used [46], incorporating the GCPs to optimize georeferencing and the quality of the generated products. RGB orthomosaics were produced, and 20 vegetation indices (VIs) commonly applied in biomass estimation were calculated, based on spectral properties related to chlorophyll content, vegetation density, and vigor [17,34,36]. Along with the VIs, individual bands (B, G, R, RE, and NIR) were also considered as predictor variables, resulting in a total of 25 spectral variables (Table S1, Supplementary Materials).

2.3.2. LiDAR Data

After the multispectral flights, the same UAV was used to acquire LiDAR data with the Zenmuse L1 sensor, which integrates a Livox LiDAR module capable of dual return, a pulse frequency of 480 kHz, and horizontal and vertical accuracies of ±5 cm and ±10 cm, respectively. Flights were conducted at an altitude of 40 m above ground level, with a speed of 4 m/s, 80% forward overlap, and 70% side overlap, parameters optimized for capturing pasture cover [33,47]. These sensor configurations and flight parameters were adjusted to maximize point cloud density and the accuracy of CHM, as recommended in previous LiDAR-based AGB studies in pastures and herbaceous vegetation [39,48].

The point clouds were processed in DJI Terra v4.0.1 (https://enterprise.dji.com/, accessed on 12 June 2025), filtering ground and vegetation returns using the Cloth Simulation Filter algorithm [49]. Easily identifiable outlier points were manually removed, while the remaining anomalies were cleaned using a statistical outlier removal tool to refine the original cloud [50], all performed in LiDAR360 v7.2.6 (https://www.greenvalleyintl.com/LiDAR360; accessed on 12 June 2025). Heights were then normalized relative to the digital terrain model (DTM), which enabled the generation of CHM; from that, a series of structural vegetation metrics were derived for AGB modeling in pastures using LiDAR data [50–52]. All point cloud processing and metric extraction were conducted using the lidR package [53] in R software (version 4.5.0) [54]. The metrics included height percentiles, mean and maximum height values, height range and standard deviation (SD), coefficient of variation (CV), kurtosis, vegetation cover, and mean intensity, among others, as described in Table S2 in the Supplementary Materials.

2.4. AGB from Field Data Collection

Given the irregular rotational grazing regime in the study sites, high spatial heterogeneity was expected; therefore, multiple quadrants per frame were sampled to capture within-plot variability, as in similar studies [15,26,36]. Following the UAV flights, five 1 × 1 m frames were placed within the subplots at each site, resulting in 30 frames in Atuen and 35 in Molinopampa (example shown in Figure 1c). In each frame, grass height was manually measured with a flexible measuring tape graduated in centimeters and millimeters (Figure 3a). AGB was collected through destructive sampling by cutting all vegetation at 2.5 cm approx. above ground level in five quadrants of 0.2 × 0.2 m, distributed across the four corners and the center of each frame. This procedure was repeated during each livestock rotation cycle. All sampling points were georeferenced using GNSS receivers in RTK mode to ensure positional accuracy and facilitate the integration of field data with UAV-derived information (Figure 3b,c).

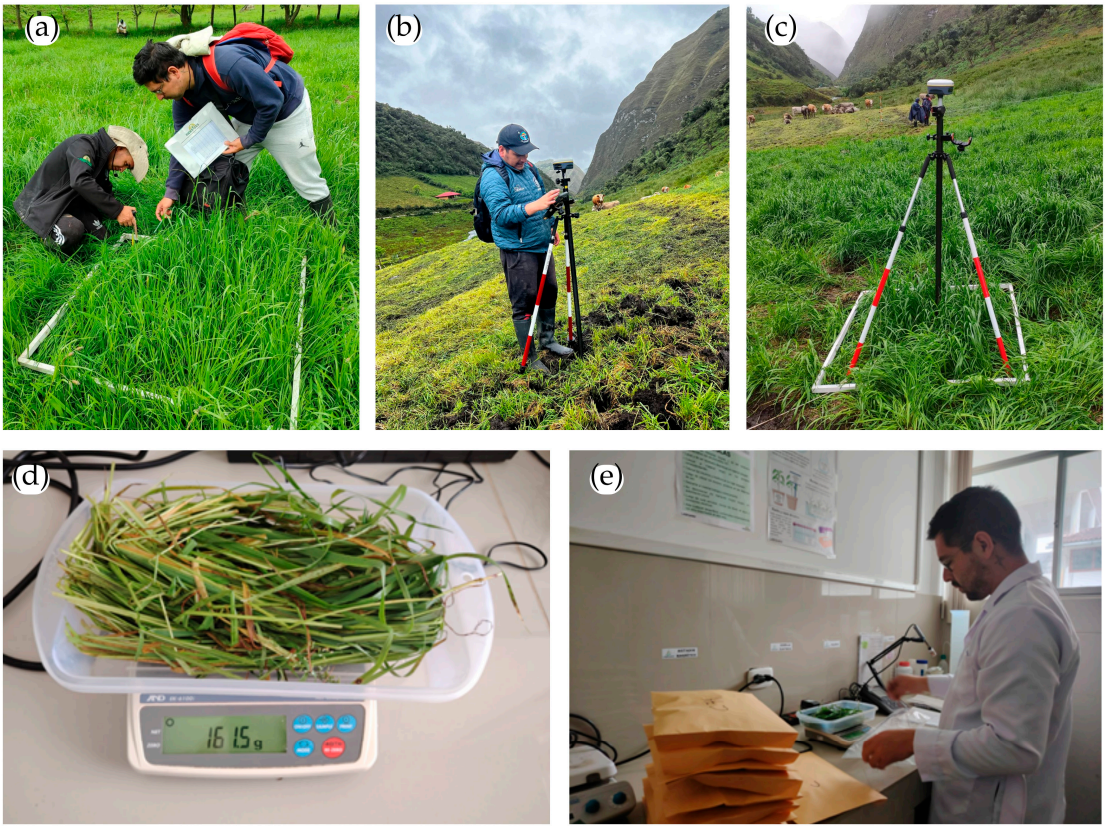

Figure 3. Procedure for aboveground biomass (AGB) collection in high-Andean pastures: (**a**) manual measurement of grass height within 1 × 1 m frames; (**b**,**c**) georeferencing of frames using GNSS receivers; (**d**,**e**) weighing of fresh samples with a digital balance and preparation for oven-drying.

Following the protocol described by Alvarez-Mendoza et al. [36], fresh samples were weighed on a digital balance to determine fresh matter (FM), then placed in paper bags and oven-dried at 60 °C for 72 h until constant weight, considered as dry matter (DM) (Figure 3d,e); FM and DM were weighed in grams. These values were summarized using descriptive statistics, and field-based AGB was aggregated to compute at site- and plot-level statistics, ensuring consistency with UAV-derived LiDAR and multispectral data across spatial resolutions.

2.5. Extraction and Integration of Spectral, Structural, and Biomass Variables

For each of the five sampling points (0.2 × 0.2 m) defined within the 1 × 1 m frames in each subplot (four corners and the center), vector masks of equal size and georeferenced location were generated using the GIS software ArcGIS Pro (version 3.1.5). These masks were applied to the multispectral orthomosaics to extract descriptive statistics (mean and standard deviation) from the RGB bands, vegetation indices, and structural metrics derived from LiDAR data. The extracted values were then linked to the corresponding field-based biomass measurements, ensuring that spectral, structural, and AGB variables were spatially and temporally aligned within each frame and subplot, thereby guaranteeing consistency for subsequent statistical analysis and modeling.

2.6. Variable Selection for Modeling

A Pearson correlation matrix was constructed, including the predictor variables (structural and spectral metrics) and the field response variables (fresh weight and dry weight). This procedure has been commonly applied in AGB estimation studies using LiDAR and multispectral data in herbaceous vegetation and pastures [34,36,51]. Variables exhibiting pairwise correlation coefficients $|r| > 0.8$ were excluded, retaining only those with lower collinearity.

2.7. AGB Modeling

Based on the previously selected spectral and structural variables, three machine learning algorithms were evaluated: Random Forest (RF) [55], Support Vector Machines (SVM) [56], and Elastic Net [57], which together provide complementary approaches for capturing the spatial variability of AGB [58,59]. Hyperparameter optimization was conducted through systematic grid search combined with five-fold cross-validation (K = 5), iteratively partitioning the dataset into training and testing subsets. This approach enabled the identification of the model with the highest predictive performance for AGB at each study site.

2.7.1. Random Forest (RF)

RF is an ensemble learning method that combines multiple decision trees to improve predictive accuracy and reduce overfitting. It has consistently shown strong performance and is among the most widely applied algorithms for AGB estimation [33,59]. The following hyperparameters were optimized: number of trees (50–1000, increments of 50), number of variables considered at each split (mtry = 5 and $n - 1$), and sampling fraction for bagging (0.1–1.0).

2.7.2. Support Vector Machines (SVM)

SVM is a supervised learning algorithm widely applied for its ability to map the variable space through kernel functions and its proven applicability in AGB estimation [60,61]. Configurations with different values of mtry, comparable to those tested in RF, were evaluated to assess the model's capacity to capture non-linear relationships between spectral and structural predictors and AGB.

2.7.3. Elastic Net

Elastic Net is a regularized regression method that combines LASSO (L1) and Ridge (L2) penalties, enabling it to handle multicollinearity while performing automatic variable selection in AGB estimation [62]. The regularization parameters α and λ were tuned through systematic grid search, and model performance was evaluated using cross-validation.

2.8. Model Evaluation

Model performance was assessed using the coefficient of determination (R^2), root mean square error (RMSE; Equation (1)) and mean absolute error (MAE; Equation (2)). These metrics are commonly used to evaluate AGB prediction models in herbaceous vegetation and grasslands using remote sensing data [36,52].

$$RMSE = \sqrt{\frac{1}{n}\sum_{i=1}^{n}(y_i - \hat{y}_i)^2} \quad (1)$$

$$MAE = \frac{1}{n}\sum_{i=1}^{n}|y_i - \hat{y}_i| \quad (2)$$

where y_i is the observed AGB of sample i, $\hat{y}_i$ is the predicted AGB, and n is the total number of samples.

3. Results

3.1. Field-Based AGB at Site and Plot Level

Field measurements revealed clear differences in AGB between sites and months (Table 1). In Atuen, mean fresh matter (FM) weight increased from 105.7 g in February to 135.7 g in March, while dry matter (DM) weight remained relatively stable (16.7–17.4 g). In Molinopampa, lower values were recorded, with FM averaging 26.3 g in March and 50.8 g in April, whereas DM increased from 4.2 g to 8.4 g over the same period. CVs at the site level were high, reaching up to 119% for FM and 115% for DM. These biomass values correspond to the 0.2 × 0.2 m sampling quadrants used for UAV-based biomass model calibration.

Table 1. Site-level summary statistics of fresh and dry AGB across sampling months (Mean and SD in grams per 0.2 × 0.2 m sampling area; CV in %).

Site	Month	AGB Type	Mean (g)	SD (g)	CV (%)	Site	Month	AGB Type	Mean (g)	SD (g)	CV (%)
Atuen	Feb.	Dry weight	16.71	8.95	53.55	Molino pampa	Mar.	Dry weight	4.15	3.27	78.82
	Feb.	Fresh weight	105.71	49.44	46.77		Mar.	Fresh weight	26.33	25.62	97.30
	Mar.	Dry weight	17.41	20.00	114.85		Apr.	Dry weight	8.37	5.00	59.73
	Mar.	Fresh weight	135.69	161.09	118.72		Apr.	Fresh weight	50.80	31.83	62.66

At the plot level, biomass measurements obtained from 0.2 × 0.2 m quadrants revealed strong within-site variability. FM ranged from 51.8 to 325.0 g in Atuen and 20.0–89.7 g in Molinopampa, while DM varied between 6.9 and 41.2 g and 2.0–14.5 g, respectively (Figure 4a–d). These ranges highlight pronounced within-site differences associated with grazing, also visible in UAV orthomosaics (Figure 4e–h). Plot-level CV values ranged from 18 to 34% in Atuen and 22–29% in Molinopampa, consistently lower than those obtained at the site scale. Detailed CV values are provided in Table S3 in the Supplementary Materials.

3.2. Correlation Between Predictor and Response Variables

The correlation analysis revealed moderate to strong associations between fresh and dry biomass and several structural and spectral predictors, although patterns varied across sites and months (Figure 5). In Atuen, February (Figure 5a) and March (Figure 5b) datasets showed positive correlations with LiDAR-derived height metrics such as the 20th (H20) and 30th (H30) height percentiles, and minimum intensity (IMIN) ($r \geq 0.5$). Chlorophyll-sensitive indices, including the Canopy Chlorophyll Content Index (CCCI) and the Green Chlorophyll Index (GCI), also exhibited consistent relationships with biomass. In Molinopampa, correlations were weaker in March (Figure 5c) but strengthened in April (Figure 5d), particularly for red-edge and chlorophyll-related indices, suggesting seasonal

shifts in predictor relevance. As expected, strong inter-correlations (r > 0.8) were observed among LiDAR height percentiles and chlorophyll indices, underscoring the need for variable reduction to mitigate multicollinearity. Overall, the analysis confirmed that both structural (LiDAR-based) and spectral (from multispectral imagery) metrics contributed to explaining AGB variability, although their predictive strength varied across sites and months.

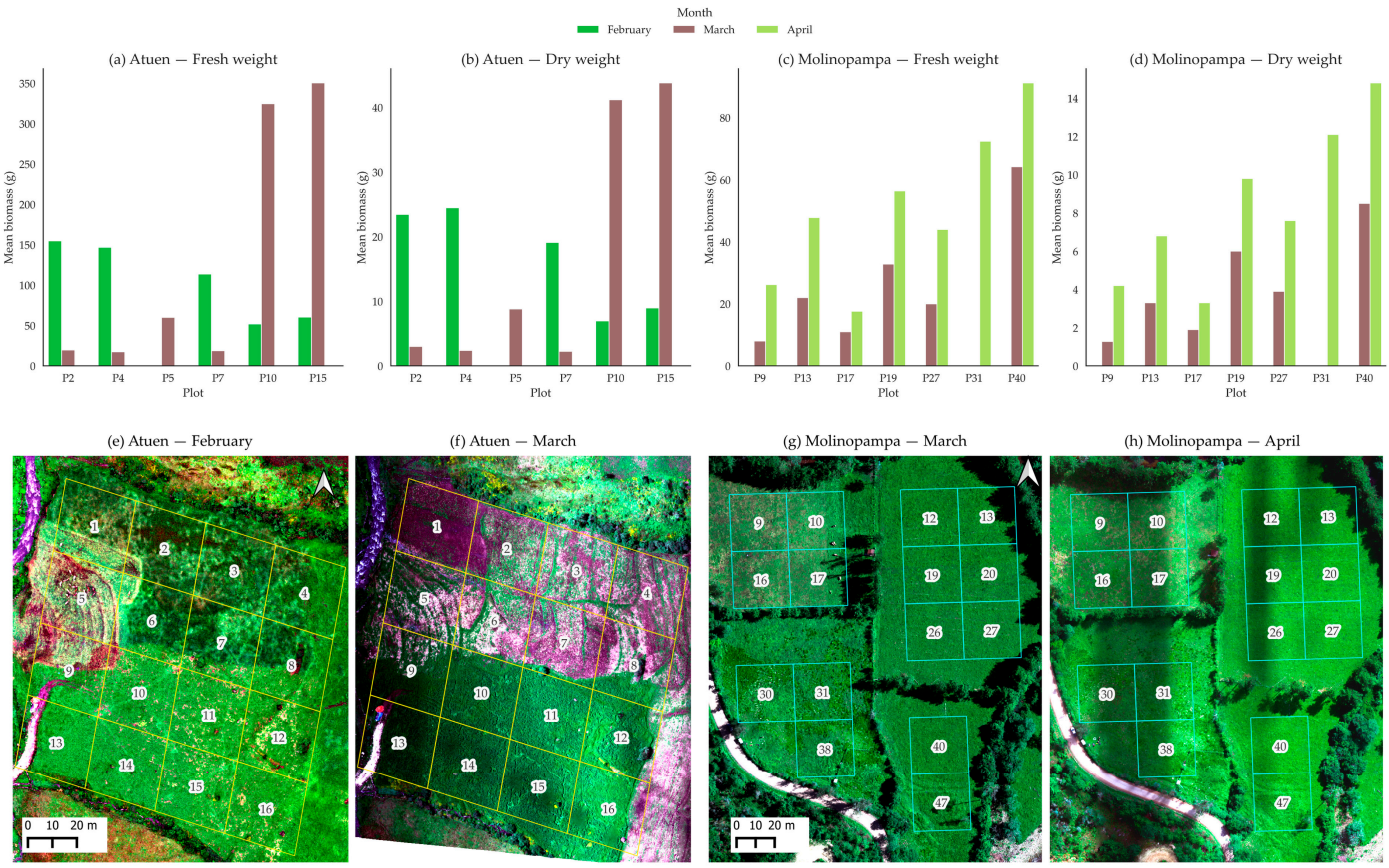

Figure 4. Plot-level variability of aboveground biomass (AGB) in Atuen and Molinopampa. Panels (**a**–**d**) present mean fresh and dry biomass per plot across months, while UAV orthomosaics (**e**–**h**) illustrate spatial heterogeneity and grazing-induced differences in grassland cover within the plots, where the numbers correspond to individual plot codes used for field biomass sampling in Atuen (**e**,**f**) and Molinopampa (**g**,**h**).

3.3. Predictive Performance of Machine Learning Models

The predictive performance of RF, SVM, and Elastic Net models for predicting fresh and dry AGB across sites and months is summarized in Table 2. Overall, RF consistently achieved the highest predictive accuracy, particularly in Atuen during March (R^2 = 0.920 for fresh biomass; R^2 = 0.903 for dry biomass). In contrast, SVM and Elastic Net performed less accurately, with Elastic Net showing the weakest results across all scenarios. In Molinopampa, RF also yielded high accuracy in both March (R^2 = 0.816 for fresh biomass; R^2 = 0.798 for dry biomass) and April, outperforming the alternative algorithms. Predictive accuracy was generally higher for dry biomass than for fresh biomass, as indicated by lower RMSE and MAE values.

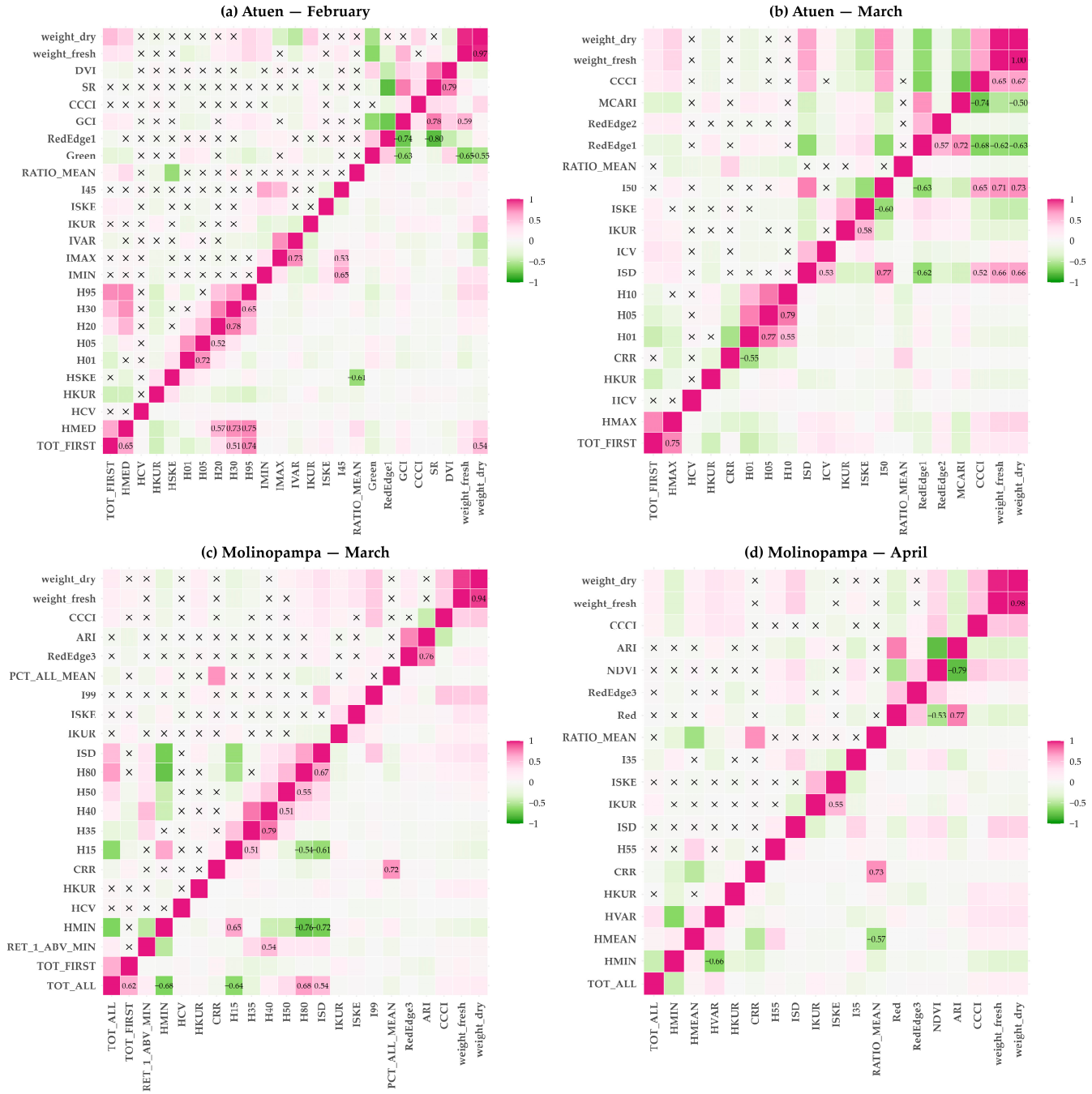

Figure 5. Pearson correlation matrices between predictor and response variables for (**a**) Atuen–February, (**b**) Atuen–March, (**c**) Molinopampa–March, and (**d**) Molinopampa–April. Significant correlations ($|r| \geq 0.5$) are shown with coefficient values, while non-significant associations ($p > 0.05$) are indicated by black "×".

Table 2. Performance metrics (R^2, MAE, RMSE) of models predicting fresh and dry AGB across sites and months.

Site—Month	Model	AGB	R^2	MAE	RMSE	Site—Month	Model	AGB	R^2	MAE	RMSE
Atuen—February	RF	Fresh	0.551	0.466	0.556	Molinopampa—March	RF	Fresh	0.624	0.397	0.812
	RF	Dry	0.561	0.087	0.094		RF	Dry	0.601	0.057	0.084
	SVM	Fresh	0.649	0.417	0.487		SVM	Fresh	0.331	0.542	1.007
	SVM	Dry	0.504	0.077	0.091		SVM	Dry	0.441	0.073	0.107
	Elastic Net	Fresh	0.567	0.45	0.552		Elastic Net	Fresh	0.332	0.608	1.019
	Elastic Net	Dry	0.446	0.085	0.097		Elastic Net	Dry	0.412	0.082	0.111

Table 2. *Cont.*

Site—Month	Model	AGB	R^2	MAE	RMSE	Site—Month	Model	AGB	R^2	MAE	RMSE
Atuen—March	RF	Fresh	0.92	1.049	1.812	Molinopampa—April	RF	Fresh	0.816	0.378	0.565
	RF	Dry	0.903	0.137	0.252		RF	Dry	0.798	0.056	0.09
	SVM	Fresh	0.858	1.671	2.386		SVM	Fresh	0.685	0.526	0.73
	SVM	Dry	0.889	0.188	0.261		SVM	Dry	0.672	0.084	0.116
	Elastic Net	Fresh	0.767	2.42	3.05		Elastic Net	Fresh	0.508	0.688	0.909
	Elastic Net	Dry	0.791	0.284	0.357		Elastic Net	Dry	0.523	0.109	0.14

3.4. Variable Importance in AGB Prediction Models

The RF models identified distinct sets of predictor variables for fresh and dry biomass estimation across sites and months (Figure 6). In Atuen, February (Figure 6a) was dominated by structural metrics such as canopy kurtosis (IKUR) and first return count (TOT_FIRST), along with chlorophyll-sensitive indices (CCCI, GCI). In March (Figure 6b), spectral indices including RedEdge1, CCCI, MCARI, and ISD became more influential. In Molinopampa, March (Figure 6c) highlighted ARI, HMIN, and CCCI as top predictors, whereas April (Figure 6d) was dominated by CCCI, RedEdge3, and NDVI. Across both sites, spectral indices consistently ranked highest, while structural LiDAR metrics showed moderate importance, reflecting the low vertical complexity of herbaceous pastures.

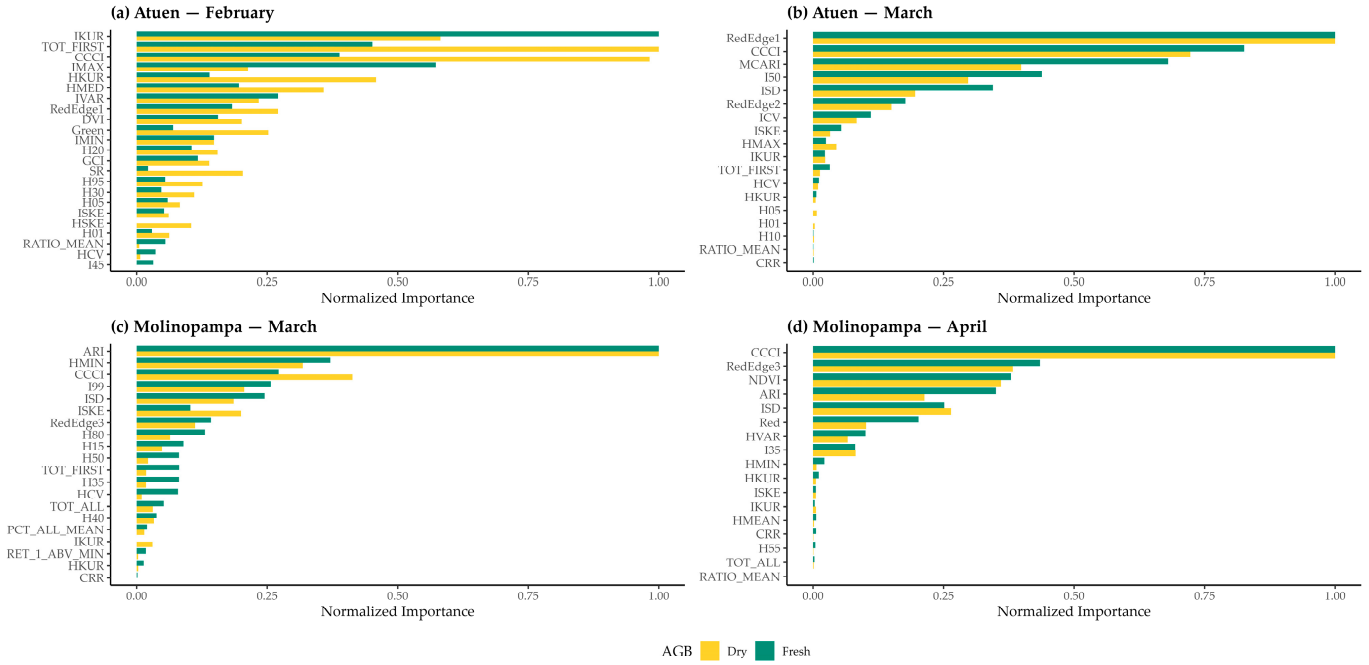

Figure 6. Normalized variable importance derived from RF models for fresh and dry AGB: (**a**) Atuen–February, (**b**) Atuen–March, (**c**) Molinopampa–March, and (**d**) Molinopampa–April.

3.5. AGB Predicted Maps

The AGB predicted values across sites, months, and spatial resolutions (0.2 m and 1 m) are summarized in Table 3, with corresponding spatial distributions shown in Figure 7.

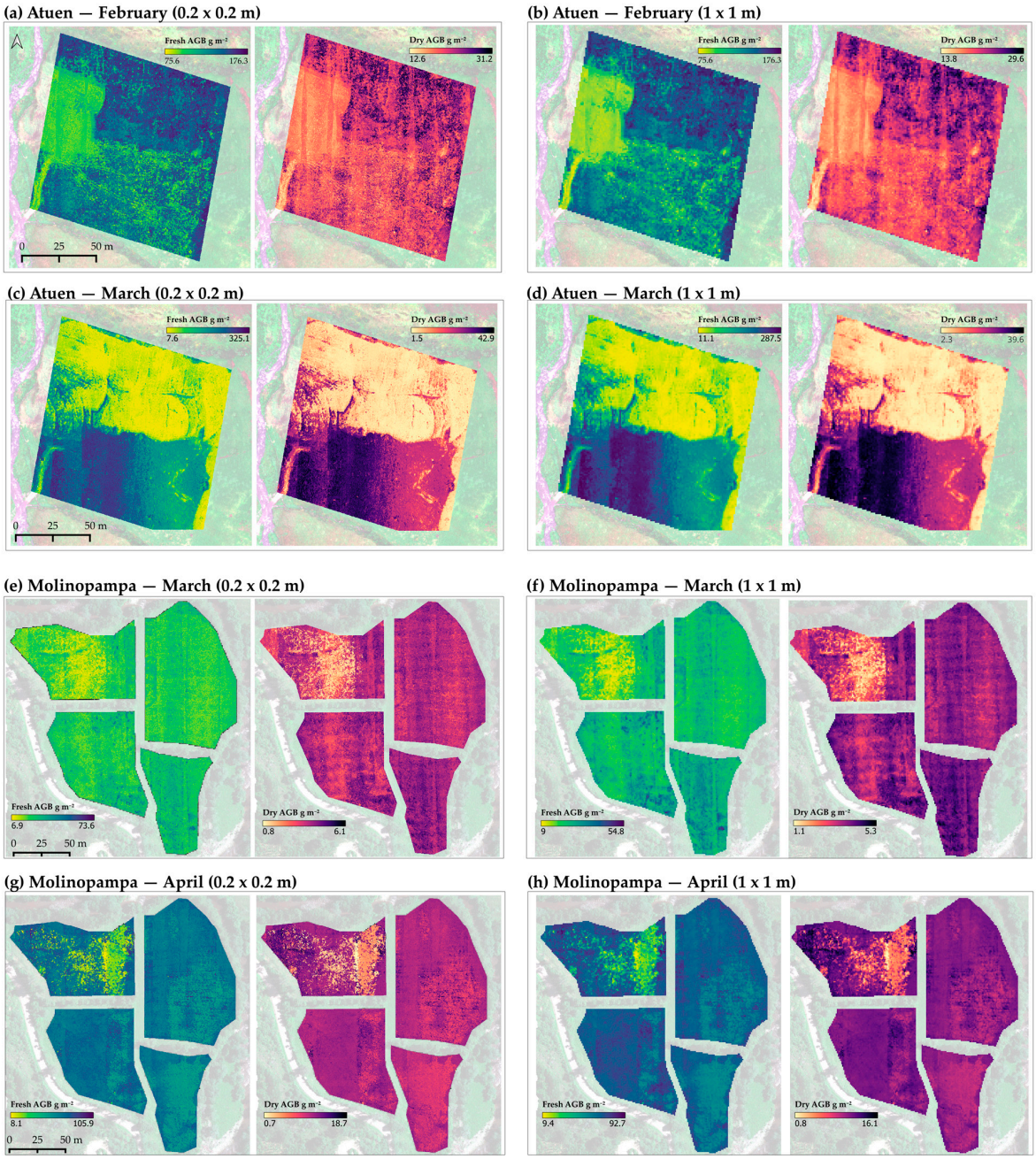

Figure 7. Predicted maps of fresh and dry AGB at two spatial resolutions (0.2 m and 1 m) across sites and months: (**a**,**b**) Atuen–February, (**c**,**d**) Atuen–March, (**e**,**f**) Molinopampa–March, and (**g**,**h**) Molinopampa–April. Values are expressed in g m^{-2}.

Table 3. Descriptive statistics of predicted fresh and dry AGB (g m^{-2}) across sites (Atuen and Molinopampa), months (February–April), and spatial resolutions (0.2 m and 1 m).

Site	Month	AGB	Spatial Resolution	Mean (±SD)	Min	Max
Atuen	February	Fresh	0.2 m	130.52 (±23.91)	75.62	176.26
		Fresh	1 m	130.64 (±19.87)	85.06	171.53
		Dry	0.2 m	20.93 (±3.54)	12.56	31.22
		Dry	1 m	20.94 (±2.74)	13.83	29.61
	March	Fresh	0.2 m	116.90 (±92.22)	7.61	325.1
		Fresh	1 m	116.95 (±89.01)	11.11	287.49
		Dry	0.2 m	16.99 (±12.69)	1.49	42.92
		Dry	1 m	17.00 (±12.24)	2.28	39.6

Table 3. *Cont.*

Site	Month	AGB	Spatial Resolution	Mean (±SD)	Min	Max
Molinopampa	March	Fresh	0.2 m	23.59 (±7.06)	6.89	73.6
		Fresh	1 m	23.65 (±5.14)	9.05	54.79
		Dry	0.2 m	3.65 (±0.77)	0.84	6.11
		Dry	1 m	3.65 (±0.62)	1.11	5.33
	April	Fresh	0.2 m	64.11 (±14.35)	8.09	105.87
		Fresh	1 m	64.23 (±10.97)	9.44	92.72
		Dry	0.2 m	10.55 (±2.41)	0.68	18.7
		Dry	1 m	10.57 (±1.76)	0.83	16.08

In Atuen, predictions revealed clear temporal and biomass-type patterns (Figure 7a–d). In February, fresh AGB ranged from 75.6 to 176.3 g m^{-2} (≈756–1763 kg ha^{-1}) and dry AGB from 12.6 to 31.2 g m^{-2} (≈126–312 kg ha^{-1}) at 0.2 m resolution, with relatively homogeneous spatial distributions (Figure 7a). By March, heterogeneity increased markedly, particularly for fresh AGB (11.1–287.5 g m^{-2}; ≈111–2875 kg ha^{-1}), with patches of high biomass interspersed with heavily grazed areas (Figure 7c). The 1 m aggregated maps (Figure 7b,d) preserved the overall spatial patterns while smoothing fine-scale variability, as indicated by lower standard deviations compared with 0.2 m products.

In Molinopampa, March maps (Figure 7e,f) showed consistently lower AGB values (fresh: 6.9–73.6 g m^{-2}; ≈69–736 kg ha^{-1}; dry: 0.8–6.1 g m^{-2}; ≈8–61 kg ha^{-1}) over large areas, reflecting the effect of continuous grazing. By April (Figure 7g,h), partial recovery was evident, with fresh AGB increasing to 9.4–105.9 g m^{-2} (≈94–1059 kg ha^{-1}) and dry AGB to 0.8–16.1 g m^{-2} (≈8–161 kg ha^{-1}). As in Atuen, the 1 m aggregated maps smoothed local heterogeneity while maintaining the main spatial gradients. Overall, these maps emphasize site- and month-specific differences in pasture productivity and the consistency between fresh and dry AGB patterns across spatial resolutions.

4. Discussion

4.1. Field-Based AGB Variability

The field-based measurements revealed pronounced spatial and temporal differences in AGB at the site level, with Atuen consistently showing higher values than Molinopampa. The high CVs observed (up to 119% for FM and 115% for DM) underscore the strong influence of grazing in shaping heterogeneity at this scale. Such variability is typical of extensively grazed pastures, where uneven regrowth arises from selective foraging, trampling, and soil pressure [63]. These processes generate patchy vegetation recovery and shifts in sward composition, amplifying biomass variability and influencing carbon stocks in tropical Andean grasslands [10,64]. Although this variability complicates model calibration, it also reflects the dynamic nature of Andean grasslands under intense grazing pressure, steep topography, and the coexistence of multiple grass species, as documented in livestock basins of the Amazon region [13,65,66].

At finer spatial scales, variability decreased. At the plot level, where five 1 × 1 m frames per plot were distributed and evaluated (Figure 1d), the CV values ranged from 18 to 34% in Atuen and 22–29% in Molinopampa. This reduction indicates that smaller sampling units capture more homogeneous conditions. Such scale-dependent effects are consistent with previous studies on AGB estimation in grasslands, which show that biomass variation diminishes when assessed within finer spatial units, but also depends on the number of replicates and the size of the sampling frames or pixel windows used [34,67]. Comparable patterns have been reported in ryegrass pastures in Ecuador, where variability was assessed in 750 m^2 plots subdivided into 0.25 m^2 subplots [15], and in Germany, where 3 × 5 m plots were evaluated under different fertilization regimes [68]. These comparisons

highlight that variability in AGB is strongly shaped by plot size, management intensity, and environmental conditions such as soil fertility and slope. In this context, our findings in Andean-Amazonian pastures, which are subject to both climatic variability and intensive grazing, reinforce the importance of explicitly considering spatial scale when linking field measurements with remote sensing predictors, since the degree of variability directly influences model calibration and predictive reliability [69,70].

4.2. Variables Correlation and Predictor Selection

The correlation analysis confirmed that LiDAR-derived structural metrics and multispectral indices provide complementary information for explaining variability in AGB. However, strong intercorrelations were observed among LiDAR height percentiles and among VIs, which risk inflating model variance and reducing interpretability. By applying a correlation threshold ($r > 0.8$), around 80% of the initial variables were eliminated, mainly redundant LiDAR percentiles and highly correlated chlorophyll indices, resulting in an optimized set of predictors consistent with recommended practices in AGB modeling [34,71]. This reduction not only improves model stability but also enhances ecological interpretability, as the retained predictors capture distinct structural or physiological processes rather than redundant information. Since AGB is strongly correlated with vegetation height, UAV-based photogrammetry and LiDAR are widely used to derive height metrics for modeling herbaceous biomass [15,52,58].

Strong associations were specifically observed for canopy height percentiles (H20, H30) and chlorophyll-sensitive indices (CCCI, GCI), consistent with evidence that structural and biochemical traits jointly regulate grassland productivity, as reflected in AGB estimates and variability of herbaceous communities derived from UAV-based LiDAR and multispectral data [34,36,52,58]. The relative contribution of these predictors, however, varied across sites and months, pointing to context-dependent drivers of biomass dynamics. In both Atuen and Molinopampa, chlorophyll indices gained importance in April, likely reflecting regrowth dynamics after grazing in combination with microclimatic conditions and livestock pressure, as previously reported in these zones [13,65,66]. These findings emphasize the importance of incorporating short-term vegetation dynamics when evaluating predictor relevance in Andean grassland ecosystems, where climate and management interact to drive rapid changes in biomass.

4.3. Model Performance and Predictor Importance

Among the tested algorithms across sites and months, RF consistently outperformed SVM and Elastic Net, achieving the highest predictive accuracy and lowest errors. Similar trends have been reported in grassland AGB modeling, where RF is widely applied either as a stand-alone method or in combination with other algorithms, often surpassing kernel-based and parametric approaches [33,34,39,52]. In some cases, alternative models such as XGBoost have shown superior results [67,70] while artificial neural networks (ANN) can outperform RF when large training datasets are available, given their capacity to capture highly complex, non-linear relationships [37]. Other studies have also highlighted the performance of algorithms such as K-Nearest Neighbor and Huber regressors, particularly when satellite-derived variables are incorporated [36]. Testing multiple algorithms is therefore crucial in heterogeneous Andean-Amazonian pastures, where predictive accuracy may depend not only on algorithmic robustness but also on sample size, predictor dimensionality, and the degree of environmental heterogeneity. In this study, predictive performance varied between fresh and dry biomass and across sites: RF achieved particularly high accuracy in Atuen during March, whereas Molinopampa showed overall lower performance, likely reflecting site-specific differences in topography, grazing intensity,

and canopy uniformity that reduce spectral separability. The weaker model performance observed in Molinopampa during February was likely due to more homogeneous pasture conditions following grazing, which lowered canopy height and spectral variability. In contrast, pasture regrowth and greater moisture availability in March increased canopy heterogeneity, enhancing the sensitivity of spectral and structural predictors to AGB.

Variable importance patterns revealed that spectral indices, particularly those related to chlorophyll content (e.g., CCCI, GCI, RedEdge), consistently dominated AGB prediction, while LiDAR-derived metrics such as canopy height and intensity percentiles contributed moderately. This dominance likely reflects the stronger sensitivity of multispectral indices to photosynthetic activity and biomass changes in short-stature pastures, where structural variability is limited. It also highlights the dual control of biomass in Andean–Amazonian pastures, where biochemical traits linked to photosynthetic activity are highly sensitive to grazing pressure, while structural attributes capture longer-term effects of trampling and regrowth [10,13,65]. Comparable patterns have been reported in tropical and highland grasslands, where the balance between spectral and structural predictors shifts according to management intensity, soil fertility, and microclimatic gradients [15,29,34]. Overall, these results highlight that variable importance is not only a statistical outcome but also an ecologically meaningful signal of how grazing and environment jointly regulate productivity in herbaceous ecosystems.

4.4. Predicted AGB and Ecological Implications

Biomass predictions revealed strong contrasts between sites. In Atuen, fresh biomass values averaged ~1300 kg ha^{-1}, with maxima up to ~3250 kg ha^{-1}, while dry biomass averaged ~210 kg ha^{-1} and reached ~430 kg ha^{-1}. These values reflect the humid conditions of the upper Utcubamba basin, where Atuen is located [72], and are consistent with yields reported for Andean ryegrass pastures in Ecuador (1471–2121 kg ha^{-1}) [15]. By contrast, in managed pastures, planted *Lolium perenne* genotypes in northern Peru have produced up to 7662 kg ha^{-1} year^{-1} of dry matter [73], highlighting the higher productivity typically achieved under fertilization and controlled management compared to extensive grazing systems. In contrast, Molinopampa showed considerably lower productivity, with fresh biomass averaging ~640 kg ha^{-1} and maxima up to ~1060 kg ha^{-1}, and dry biomass peaking at ~190 kg ha^{-1}. These lower values, compared with Atuen, likely reflect differences in grazing pressure, soil fertility, and species composition in the herbaceous layer reported for Molinopampa sector [41,66]. In addition, local climate and management practices strongly affect vegetation recovery and biomass accumulation. Atuen benefits from cooler and more humid conditions that favor pasture regrowth, whereas in Molinopampa, higher grazing intensity and drier microclimatic conditions may limit vegetation recovery and increase spatial variability in AGB. Together, these findings emphasize the influence of site-specific conditions: climate, topography, and management in shaping biomass dynamics in tropical Andean pastures [10]. Comparable patterns linking grazing management, soil fertility, and biomass productivity have been reported in tropical and high-Andean grasslands [15,29,36].

Related to AGB mapping and spatial resolution, fine-scale products (0.2 m) captured localized grazing scars and depletion zones, whereas aggregation to 1 m reduced local variability but preserved broader spatial gradients. Similar patterns have been reported even at coarser scales (up to 10 m) when UAV-derived AGB data were aggregated for grassland monitoring [52]. This scaling effect underscores the capacity of UAV-based approaches to detect grazing impacts at fine resolution while generating products that remain consistent and comparable at coarser levels, as demonstrated in other grassland ecosystems [38,74,75]. From a management perspective, fine-scale maps are ideal for as-

sessing localized degradation, forage availability, and vegetation recovery within pastures, whereas coarser resolutions are valuable for extending monitoring to provincial or regional levels and supporting land-use planning [65]. Moreover, UAV-derived AGB products can serve as training data to facilitate upscaling and promote multi-scale grassland monitoring, providing information relevant to different decision-making levels in grazing and watershed management.

4.5. Limitations and Future Perspectives

This study provides robust empirical evidence for the potential of integrating UAV-based LiDAR and multispectral data in estimating AGB in Andean–Amazonian pastures in the Amazonas department, offering one of the first spatially explicit assessments of biomass dynamics in these highly heterogeneous grazing systems. Some limitations must be acknowledged: the short monitoring period restricted the assessment of longer-term dynamics, the limited number of plots reduced representativeness at broader scales, and unmeasured factors such as pasture composition and management history likely contributed to site-specific variability. In addition, soil fertility was not directly measured, which may partly explain the observed differences in pasture productivity between sectors. Furthermore, as the observations covered only two months, the models capture a short-term snapshot of pasture conditions; therefore, their applicability to other months or years requires further validation under varying climatic conditions. Even so, this work establishes a pioneering framework for multi-scale biomass monitoring, offering a methodological framework for more robust and scalable approaches in tropical highland pastures.

5. Conclusions

This study demonstrates the potential of integrating UAV-based LiDAR and multispectral data for estimating AGB in Andean–Amazonian pastures of northern Peru, providing one of the first spatially explicit assessments of these ecosystems under extensive grazing. The approach captured grazing-induced heterogeneity at fine spatial scales while preserving broader structural gradients, underscoring the value of multi-scale analyses for understanding biomass dynamics in highly variable highland pastures.

This research establishes a pioneering framework for AGB monitoring in tropical highland pastures, despite limitations related to monitoring duration, sample size, and UAV coverage. The consistency of predicted values with regional studies in Ecuador and Peru supports the reliability of the approach and its potential for broader application. Future work should extend monitoring over longer periods and integrate UAV data with satellite time series to enable regional upscaling, while incorporating environmental and management variables to refine ecological interpretation. Overall, the framework presented here offers a scalable tool for quantifying forage availability, supporting adaptive grazing strategies, and guiding sustainable management of high-altitude grasslands in Andean–Amazonian ecosystems.

Supplementary Materials: The following supporting information can be downloaded at: https://www.mdpi.com/article/10.3390/su17219745/s1. Table S1: Vegetation indices (VIs) derived from UAV multispectral imagery, applied to aboveground biomass (AGB) estimation [76–95]; Table S2: LiDAR structural metrics used for AGB estimation, grouped into point count, height, intensity, percentile, and ratio/threshold metrics; Table S3: Plot-level statistics of fresh and dry AGB by month, including sample size (count), mean, standard deviation (SD), and coefficient of variation (CV).

Author Contributions: Conceptualization, A.J.M.-M. and A.C.-S.; methodology, A.J.M.-M., S.P., K.M.T.-T., J.A.Z.-S., A.S.R.-F., J.O.S.-L., R.S.L., J.A.S.-V., T.B.S.-M., M.O.-C., R.E.T.M., E.B. and A.C.-S.; software, A.J.M.-M. and S.P.; validation, A.J.M.-M. and K.M.T.-T.; formal analysis, A.J.M.-M., S.P. and A.C.-S.; investigation, A.J.M.-M., S.P., K.M.T.-T., J.A.Z.-S., A.S.R.-F., J.O.S.-L., R.S.L., J.A.S.-V.,

T.B.S.-M., M.O.-C., R.E.T.M., E.B. and A.C.-S.; data curation, S.P., A.S.R.-F., J.A.S.-V. and A.C.-S.; writing—original draft preparation, A.J.M.-M.; writing—review and editing, K.M.T.-T., J.A.Z.-S., J.O.S.-L., T.B.S.-M. and A.C.-S.; visualization, A.J.M.-M., S.P., J.A.Z.-S. and R.E.T.M.; supervision, A.C.-S.; project administration, R.S.L., M.O.-C. and E.B.; funding acquisition, A.J.M.-M. and A.C.-S. All authors have read and agreed to the published version of the manuscript.

Funding: This research was funded by CONCYTEC through the PROCIENCIA, grant number CONTRATO N° PE501087299-2024-PROCIENCIA. Proyecto "Desarrollo de una metodología de estimación de biomasa en especies cespitosas mediante Lidar y UAV, en zonas altoandinas de la región Amazonas"—LIDARPAS.

Institutional Review Board Statement: Not applicable.

Informed Consent Statement: Not applicable.

Data Availability Statement: The data used in this study are available on request from the first and corresponding author.

Acknowledgments: We would like to express our sincere gratitude to the Research Institute for Sustainable Development of Ceja de Selva (INDES-CES) of the Toribio Rodríguez de Mendoza National University in Amazonas, for providing the necessary facilities to conduct this research.

Conflicts of Interest: Author Renzo E. Terrones Murga was employed by the company Lidar Peru Sociedad Cerrada. The remaining authors declare that the research was conducted in the absence of any commercial or financial relationships that could be construed as a potential conflict of interest.

References

1. O'Mara, F.P. The Role of Grasslands in Food Security and Climate Change. *Ann. Bot.* **2012**, *110*, 1263–1270. [CrossRef]
2. White, R.P.; Murray, S.; Rohweder, M.; Prince, S.D.; Thompson, K.M. *Grassland Ecosystems*; World Resources Institute: Washington, DC, USA, 2000.
3. Petermann, J.S.; Buzhdygan, O.Y. Grassland Biodiversity. *Curr. Biol.* **2021**, *31*, R1195–R1201. [CrossRef]
4. Scurlock, J.M.O.; Hall, D.O. The Global Carbon Sink: A Grassland Perspective. *Glob. Change Biol.* **1998**, *4*, 229–233. [CrossRef]
5. Török, P.; Brudvig, L.A.; Kollmann, J.; Price, J.N.; Tóthmérész, B. The Present and Future of Grassland Restoration. *Restor. Ecol.* **2021**, *29*, e13378. [CrossRef]
6. MINAGRI Minagri Instalará Más de 128 000 Hectáreas de Pastos Para Impulsar Producción Ganadera en Zonas Rurales. Available online: https://www.gob.pe/institucion/agrorural/noticias/526008-minagri-instalara-mas-de-128-000-hectareas-de-pastos-para-impulsar-produccion-ganadera-en-zonas-rurales (accessed on 11 August 2025).
7. Fuentes, E.; Gómez, C.; Pizarro, D.; Alegre, J.; Castillo, M.; Vela, J.; Huaman, E.; Vásquez, H. A Review of Silvopastoral Systems in the Peruvian Amazon Region. *Trop. Grassl.-Forrajes Trop.* **2022**, *10*, 78–88. [CrossRef]
8. Raul Marino, Y.C.; Ja, O.; Se, P. Species of the Poaceae Family Suitable for Andean Livestock Farming in the Peruvian Andes Reported in GBIF and Local Studies. *Glob. J. Ecol.* **2024**, *9*, 057–065. [CrossRef]
9. Medina Quispe, P.R.; Arizapana-Almonacid, M.A.; Nosetto, M.D. Changes in the Soil Organic Carbon of Grasslands in the High Andes of Peru after Their Conversion to Croplands and Their Environmental Controls. *Grasses* **2024**, *3*, 35–44. [CrossRef]
10. Duchicela, S.A.; Llambí, L.D.; Bonnesoeur, V.; Román-Dañobeytia, F. Pastoralism in the High Tropical Andes: A Review of the Effect of Grazing Intensity on Plant Diversity and Ecosystem Services. *Appl. Veg. Sci.* **2024**, *27*, e12791. [CrossRef]
11. Taboada-Hermoza, R.; Martínez, A.G. "No One Is Safe": Agricultural Burnings, Wildfires and Risk Perception in Two Agropastoral Communities in the Puna of Cusco, Peru. *Fire* **2025**, *8*, 60. [CrossRef]
12. Cervantes, R.; Sánchez, J.M.; Alegre, J.; Rendón, E.; Baiker, J.R.; Locatelli, B.; Bonnesoeur, V. Contribución de Los Ecosistemas Altoandinos En La Provisión Del Servicio Ecosistémico de Regulación Hídrica. *Ecol. Apl.* **2022**, *20*, 137–146. [CrossRef]
13. Vásquez, H.V.; Huamán Puscán, M.M.; Bobadilla, L.G.; Zagaceta, H.; Valqui, L.; Maicelo, J.L.; Silva-López, J.O. Evaluation of Pasture Degradation through Vegetation Indices of the Main Livestock Micro-Watersheds in the Amazon Region (NW Peru). *Environ. Sustain. Indic.* **2023**, *20*, 100315. [CrossRef]
14. Ramos-Hernández, E.; Martínez Sánchez, J.L. Almacenes de Biomasa y Carbono Aéreo y Radicular En Pastizales de Urochloa Decumbens y Paspalum Notatum (Poaceae) En El Sureste de México. *RBT* **2020**, *68*, 440–451. [CrossRef]
15. Sinde-González, I.; Gil-Docampo, M.; Arza-García, M.; Grefa-Sánchez, J.; Yánez-Simba, D.; Pérez-Guerrero, P.; Abril-Porras, V. Biomass Estimation of Pasture Plots with Multitemporal UAV-Based Photogrammetric Surveys. *Int. J. Appl. Earth Obs. Geoinf.* **2021**, *101*, 102355. [CrossRef]

16. Segura-Carmona, J.E.; Yerena Yamallel, J.I.; Bernal Barragán, H.; Alanís Rodríguez, E.; Cuéllar Rodríguez, L.G.; Jiménez Pérez, J. Generación de Nuevas Ecuaciones Para Estimar La Biomasa Aérea a Partir de Variables Morfológicas Obtenidas de Pastos En Agostaderos de Nuevo León, México. *Rev. Mex. Cienc. Pecu.* **2024**, *15*, 1–16. [CrossRef]
17. Tong, X.; Duan, L.; Liu, T.; Yang, Z.; Wang, Y.; Singh, V.P. Estimation of Grassland Aboveground Biomass Combining Optimal Derivative and Raw Reflectance Vegetation Indices at Peak Productive Growth Stage. *Geocarto Int.* **2023**, *38*, 2186497. [CrossRef]
18. Waite, R.B. The Application of Visual Estimation Procedures for Monitoring Pasture Yield and Composition in Exclosures and Small Plots. *Trop. Grassl.* **1994**, *28*, 38.
19. Archibald, S.; Bond, W.J.; Stock, W.D.; Fairbanks, D.H.K. Shaping the Landscape: Fire–Grazer Interactions in an African Savanna. *Ecol. Appl.* **2005**, *15*, 96–109. [CrossRef]
20. Joubert, D.; Powell, L.A.; Schacht, W.H. Visual Obstruction as a Method to Quantify Herbaceous Biomass in Southern African Semi-Arid Savannas. *Afr. J. Range Forage Sci.* **2015**, *32*, 225–230. [CrossRef]
21. Riginos, C.; Grace, J.B.; Augustine, D.J.; Young, T.P. Local versus Landscape-scale Effects of Savanna Trees on Grasses. *J. Ecol.* **2009**, *97*, 1337–1345. [CrossRef]
22. Ali, I.; Cawkwell, F.; Dwyer, E.; Barrett, B.; Green, S. Satellite Remote Sensing of Grasslands: From Observation to Management. *J. Plant Ecol.* **2016**, *9*, 649–671. [CrossRef]
23. Reinermann, S.; Asam, S.; Kuenzer, C. Remote Sensing of Grassland Production and Management—A Review. *Remote Sens.* **2020**, *12*, 1949. [CrossRef]
24. Crabbe, R.A.; Lamb, D.W.; Edwards, C.; Andersson, K.; Schneider, D. A Preliminary Investigation of the Potential of Sentinel-1 Radar to Estimate Pasture Biomass in a Grazed Pasture Landscape. *Remote Sens.* **2019**, *11*, 872. [CrossRef]
25. Chen, Y.; Guerschman, J.; Shendryk, Y.; Henry, D.; Harrison, M.T. Estimating Pasture Biomass Using Sentinel-2 Imagery and Machine Learning. *Remote Sens.* **2021**, *13*, 603. [CrossRef]
26. Wang, J.; Xiao, X.; Bajgain, R.; Starks, P.; Steiner, J.; Doughty, R.B.; Chang, Q. Estimating Leaf Area Index and Aboveground Biomass of Grazing Pastures Using Sentinel-1, Sentinel-2 and Landsat Images. *ISPRS J. Photogramm. Remote Sens.* **2019**, *154*, 189–201. [CrossRef]
27. Zhang, B.; Zhang, L.; Xie, D.; Yin, X.; Liu, C.; Liu, G. Application of Synthetic NDVI Time Series Blended from Landsat and MODIS Data for Grassland Biomass Estimation. *Remote Sens.* **2015**, *8*, 10. [CrossRef]
28. Anaya, J.A.; Chuvieco, E.; Palacios-Orueta, A. Aboveground Biomass Assessment in Colombia: A Remote Sensing Approach. *For. Ecol. Manag.* **2009**, *257*, 1237–1246. [CrossRef]
29. Nuñez Delgado, J.; Pizarro Carcausto, S.; Gutiérrez Tang, M.; Ñaupari Vásquez, J. Dinámica Espacio Temporal de La Biomasa Aérea En Pastizales Altoandinos Basado En NDVI-MODIS Validado Por Espectrometría in Situ. *Rev. Investig. Vet. Perú* **2021**, *32*, e20392. [CrossRef]
30. Bendix, J.; Rollenbeck, R.; Göttlicher, D.; Cermak, J. Cloud Occurrence and Cloud Properties in Ecuador. *Clim. Res.* **2006**, *30*, 133–147. [CrossRef]
31. Montenegro-Díaz, P.; Alvear, R.C.; Carrillo-Rojas, G. Overcast Sky Condition Prevails on and Influences the Biometeorology of the Tropical Andean Páramos. *J. Mt. Sci.* **2023**, *20*, 78–86. [CrossRef]
32. Santos, W.M.D.; Martins, L.D.C.D.S.; Bezerra, A.C.; Souza, L.S.B.D.; Jardim, A.M.D.R.F.; Silva, M.V.D.; Souza, C.A.A.D.; Silva, T.G.F.D. Use of Unmanned Aerial Vehicles for Monitoring Pastures and Forages in Agricultural Sciences: A Systematic Review. *Drones* **2024**, *8*, 585. [CrossRef]
33. Bazzo, C.O.G.; Kamali, B.; Hütt, C.; Bareth, G.; Gaiser, T. A Review of Estimation Methods for Aboveground Biomass in Grasslands Using UAV. *Remote Sens.* **2023**, *15*, 639. [CrossRef]
34. Freitas, R.G.; Pereira, F.R.S.; Dos Reis, A.A.; Magalhães, P.S.G.; Figueiredo, G.K.D.A.; Do Amaral, L.R. Estimating Pasture Aboveground Biomass under an Integrated Crop-Livestock System Based on Spectral and Texture Measures Derived from UAV Images. *Comput. Electron. Agric.* **2022**, *198*, 107122. [CrossRef]
35. Zhang, H.; Tang, Z.; Wang, B.; Meng, B.; Qin, Y.; Sun, Y.; Lv, Y.; Zhang, J.; Yi, S. A Non-Destructive Method for Rapid Acquisition of Grassland Aboveground Biomass for Satellite Ground Verification Using UAV RGB Images. *Glob. Ecol. Conserv.* **2022**, *33*, e01999. [CrossRef]
36. Alvarez-Mendoza, C.I.; Guzman, D.; Casas, J.; Bastidas, M.; Polanco, J.; Valencia-Ortiz, M.; Montenegro, F.; Arango, J.; Ishitani, M.; Selvaraj, M.G. Predictive Modeling of Above-Ground Biomass in Brachiaria Pastures from Satellite and UAV Imagery Using Machine Learning Approaches. *Remote Sens.* **2022**, *14*, 5870. [CrossRef]
37. Vahidi, M.; Shafian, S.; Thomas, S.; Maguire, R. Pasture Biomass Estimation Using Ultra-High-Resolution RGB UAVs Images and Deep Learning. *Remote Sens.* **2023**, *15*, 5714. [CrossRef]
38. Michez, A.; Lejeune, P.; Bauwens, S.; Herinaina, A.; Blaise, Y.; Castro Muñoz, E.; Lebeau, F.; Bindelle, J. Mapping and Monitoring of Biomass and Grazing in Pasture with an Unmanned Aerial System. *Remote Sens.* **2019**, *11*, 473. [CrossRef]
39. Hütt, C.; Isselstein, J.; Komainda, M.; Schöttker, O.; Sturm, A. UAV LiDAR-Based Grassland Biomass Estimation for Precision Livestock Management. *J. Appl. Remote Sens.* **2024**, *18*, 017502. [CrossRef]

40. Urquizo, J.; Ccopi, D.; Ortega, K.; Castañeda, I.; Patricio, S.; Passuni, J.; Figueroa, D.; Enriquez, L.; Ore, Z.; Pizarro, S. Estimation of Forage Biomass in Oat (Avena Sativa) Using Agronomic Variables through UAV Multispectral Imaging. *Remote Sens.* **2024**, *16*, 3720. [CrossRef]
41. Bobadilla Rivera, L.G.; Chichipe Vela, E.; Oliva, M. Efecto de Cuatro Enmiendas Cálcicas Sobre El Suelo En El Rendimiento de Cinco Especies Forrajeras Presentes En El Distrito de Molinopampa (Región Amazonas). *Rev. Investig. Agroprod. Sustent.* **2018**, *2*, 7–13. [CrossRef]
42. Murga, L.; Vásquez, H.; Bardales, J. Caracterización de Los Sistemas de Producción de Ganado Bovino En Las Cuencas Ganaderas de Ventilla, Florida y Leyva -Región Amazonas. *Rev. Científica UNTRM Cienc. Nat. E Ing.* **2019**, *1*, 28–37. [CrossRef]
43. SENAMHI SENAMHI-Estaciones. Available online: https://www.senamhi.gob.pe/?p=estaciones (accessed on 16 September 2025).
44. MicaSense RedEdge-MX Integration Guide. Available online: https://support.micasense.com/hc/en-us/articles/360011389334-RedEdge-MX-Integration-Guide (accessed on 16 September 2025).
45. Newell, F.L.; Ausprey, I.J.; Robinson, S.K. Spatiotemporal Climate Variability in the Andes of Northern Peru: Evaluation of Gridded Datasets to Describe Cloud Forest Microclimate and Local Rainfall. *Int. J. Climatol.* **2022**, *42*, 5892–5915. [CrossRef]
46. PIX4Dmapper 2025. Available online: https://support.pix4d.com/ (accessed on 29 October 2025).
47. Eskandari, R.; Mahdianpari, M.; Mohammadimanesh, F.; Salehi, B.; Brisco, B.; Homayouni, S. Meta-Analysis of Unmanned Aerial Vehicle (UAV) Imagery for Agro-Environmental Monitoring Using Machine Learning and Statistical Models. *Remote Sens.* **2020**, *12*, 3511. [CrossRef]
48. Poley, L.G.; McDermid, G.J. A Systematic Review of the Factors Influencing the Estimation of Vegetation Aboveground Biomass Using Unmanned Aerial Systems. *Remote Sens.* **2020**, *12*, 1052. [CrossRef]
49. Zhang, W.; Qi, J.; Wan, P.; Wang, H.; Xie, D.; Wang, X.; Yan, G. An Easy-to-Use Airborne LiDAR Data Filtering Method Based on Cloth Simulation. *Remote Sens.* **2016**, *8*, 501. [CrossRef]
50. Chen, A.; Wang, X.; Zhang, M.; Guo, J.; Xing, X.; Yang, D.; Zhang, H.; Hou, Z.; Jia, Z.; Yang, X. Fusion of LiDAR and Multispectral Data for Aboveground Biomass Estimation in Mountain Grassland. *Remote Sens.* **2023**, *15*, 405. [CrossRef]
51. Da Costa, M.B.T.; Silva, C.A.; Broadbent, E.N.; Leite, R.V.; Mohan, M.; Liesenberg, V.; Stoddart, J.; Do Amaral, C.H.; De Almeida, D.R.A.; Da Silva, A.L.; et al. Beyond Trees: Mapping Total Aboveground Biomass Density in the Brazilian Savanna Using High-Density UAV-Lidar Data. *For. Ecol. Manag.* **2021**, *491*, 119155. [CrossRef]
52. Liu, B.; Ye, H.; Liao, X.; Zhang, X.; Mao, G.; Pan, T. UAV Data for Herbaceous Community' Aboveground Biomass Upscaling: A New Perspective on LiDAR and Multispectral Information Fusion. *Int. J. Digit. Earth* **2025**, *18*, 2543563. [CrossRef]
53. Roussel, J.-R.; Auty, D.; Coops, N.C.; Tompalski, P.; Goodbody, T.R.H.; Meador, A.S.; Bourdon, J.-F.; De Boissieu, F.; Achim, A. lidR: An R Package for Analysis of Airborne Laser Scanning (ALS) Data. *Remote Sens. Environ.* **2020**, *251*, 112061. [CrossRef]
54. R Core Team R. *A Language and Environment for Statistical Computing*; R Core Team R: Vienna, Austria, 2025.
55. Breiman, L. Random Forests. *Mach. Learn.* **2001**, *45*, 5–32. [CrossRef]
56. Cortes, C.; Vapnik, V. Support-Vector Networks. *Mach. Learn.* **1995**, *20*, 273–297. [CrossRef]
57. Zou, H.; Hastie, T. Regularization and Variable Selection Via the Elastic Net. *J. R. Stat. Soc. Ser. B Stat. Methodol.* **2005**, *67*, 301–320. [CrossRef]
58. Coverdale, T.C.; Boucher, P.B.; Singh, J.; Davies, A.B. Quantifying Aboveground Herbaceous Biomass in Grassy Ecosystems: A Comparison of Field and High-resolution UAV-LiDAR Approaches. *Remote Sens. Ecol. Conserv.* **2025**, rse2.70023. [CrossRef]
59. Liu, W.; Xu, C.; Zhang, Z.; De Boeck, H.; Wang, Y.; Zhang, L.; Xu, X.; Zhang, C.; Chen, G.; Xu, C. Machine Learning-Based Grassland Aboveground Biomass Estimation and Its Response to Climate Variation in Southwest China. *Front. Ecol. Evol.* **2023**, *11*, 1146850. [CrossRef]
60. Hao, L.; Ye, H.; He, S.; Zhang, X.; Bayin, D.; Safarov, M.; Okhonniyozov, M.; Liao, X. Estimation of Aboveground Biomass in Tajikistan Based on Upscaling Extrapolation of UAV and Sentinel-2 Multi-Source Data Synergy. *Sci. Remote Sens.* **2025**, *12*, 100259. [CrossRef]
61. Huang, W.; Li, W.; Xu, J.; Ma, X.; Li, C.; Liu, C. Hyperspectral Monitoring Driven by Machine Learning Methods for Grassland Above-Ground Biomass. *Remote Sens.* **2022**, *14*, 2086. [CrossRef]
62. Chen, D.; Luo, H.; Liu, Z.; Pan, J.; Wu, Y.; Wang, E.; Lu, C.; Wang, L.; Wang, W.; Ou, G. A Dual-Variable Selection Framework for Enhancing Forest Aboveground Biomass Estimation via Multi-Source Remote Sensing. *Remote Sens.* **2025**, *17*, 2493. [CrossRef]
63. Fraser, M.D.; Vallin, H.E.; Roberts, B.P. Animal Board Invited Review: Grassland-Based Livestock Farming and Biodiversity. *animal* **2022**, *16*, 100671. [CrossRef]
64. Oliveras, I.; Girardin, C.; Doughty, C.E.; Cahuana, N.; Arenas, C.E.; Oliver, V.; Huaraca Huasco, W.; Malhi, Y. Andean Grasslands Are as Productive as Tropical Cloud Forests. *Environ. Res. Lett.* **2014**, *9*, 115011. [CrossRef]
65. Marin, N.A.; Barboza, E.; López, R.S.; Vásquez, H.V.; Gómez Fernández, D.; Terrones Murga, R.E.; Rojas Briceño, N.B.; Oliva-Cruz, M.; Gamarra Torres, O.A.; Silva López, J.O.; et al. Spatiotemporal Dynamics of Grasslands Using Landsat Data in Livestock Micro-Watersheds in Amazonas (NW Peru). *Land* **2022**, *11*, 674. [CrossRef]

66. Oliva, M.; Rojas, D.; Morales, A.; Oliva, C.; Oliva, M.A. Nutritional Content, Digestibility and Performance of Native Grasses Biomass That Dominate Livestock Molinopampa, Pomacochas and Leymebamba Basins, Amazonas, Peru. *Sci. Agropecu.* **2015**, *6*, 211–215. [CrossRef]
67. Dos Reis, A.A.; Werner, J.P.S.; Silva, B.C.; Figueiredo, G.K.D.A.; Antunes, J.F.G.; Esquerdo, J.C.D.M.; Coutinho, A.C.; Lamparelli, R.A.C.; Rocha, J.V.; Magalhães, P.S.G. Monitoring Pasture Aboveground Biomass and Canopy Height in an Integrated Crop–Livestock System Using Textural Information from PlanetScope Imagery. *Remote Sens.* **2020**, *12*, 2534. [CrossRef]
68. Lussem, U.; Schellberg, J.; Bareth, G. Monitoring Forage Mass with Low-Cost UAV Data: Case Study at the Rengen Grassland Experiment. *PFG* **2020**, *88*, 407–422. [CrossRef]
69. Cai, T.; Chang, C.; Zhao, Y.; Wang, X.; Yang, J.; Dou, P.; Otgonbayar, M.; Zhang, G.; Zeng, Y.; Wang, J. Within-Season Estimates of 10 m Aboveground Biomass Based on Landsat, Sentinel-2 and PlanetScope Data. *Sci Data* **2024**, *11*, 1276. [CrossRef] [PubMed]
70. Chen, A.; Xu, C.; Zhang, M.; Guo, J.; Xing, X.; Yang, D.; Xu, B.; Yang, X. Cross-Scale Mapping of above-Ground Biomass and Shrub Dominance by Integrating UAV and Satellite Data in Temperate Grassland. *Remote Sens. Environ.* **2024**, *304*, 114024. [CrossRef]
71. Maesano, M.; Khoury, S.; Nakhle, F.; Firrincieli, A.; Gay, A.; Tauro, F.; Harfouche, A. UAV-Based LiDAR for High-Throughput Determination of Plant Height and Above-Ground Biomass of the Bioenergy Grass Arundo Donax. *Remote Sens.* **2020**, *12*, 3464. [CrossRef]
72. Rivera-Fernandez, A.; Cotrina-Sanchez, A.; Salas López, R.; Zabaleta-Santisteban, J.; Rios, N.; Medina-Medina, A.; Tuesta-Trauco, K.; Sánchez-Vega, J.; Silva-Melendez, T.; Oliva-Cruz, M.; et al. Spatiotemporal Land Cover Change and Future Hydrological Impacts Under Climate Scenarios in the Amazonian Andes: A Case Study of the Utcubamba River Basin. *Land* **2025**, *14*, 1234. [CrossRef]
73. Vallejos-Fernández, L.A.; Alvarez, W.Y.; Paredes-Arana, M.E.; Pinares-Patiño, C.; Bustíos-Valdivia, J.C.; Vásquez, H.; García-Ticllacuri, R. Productive Behavior and Nutritional Value of 22 Genotypes of Ryegrass (*Lolium* spp.) on Three High Andean Floors of Northern Peru. *Sci. Agropecu.* **2020**, *11*, 537–545. [CrossRef]
74. Barnetson, J.; Phinn, S.; Scarth, P. Estimating Plant Pasture Biomass and Quality from UAV Imaging across Queensland's Rangelands. *AgriEngineering* **2020**, *2*, 523–543. [CrossRef]
75. Lyu, X.; Li, X.; Dang, D.; Dou, H.; Wang, K.; Lou, A. Unmanned Aerial Vehicle (UAV) Remote Sensing in Grassland Ecosystem Monitoring: A Systematic Review. *Remote Sens.* **2022**, *14*, 1096. [CrossRef]
76. Rouse, J.W.; Hass, R.H.; Schell, J.A.; Deering, D.W. Monitoring Vegetation Systems in the Great Plains with ERTS. In Proceedings of the Earth Resources Technology Satellite Symposium, Washington, DC, USA, 10–14 December 1973; Volume 1, pp. 309–317.
77. Gitelson, A.; Merzlyak, M.N. Spectral Reflectance Changes Associated with Autumn Senescence of Aesculus Hippocastanum L. and Acer Platanoides L. Leaves. Spectral Features and Relation to Chlorophyll Estimation. *J. Plant Physiol.* **1994**, *143*, 286–292. [CrossRef]
78. Gitelson, A.A.; Kaufman, Y.J.; Merzlyak, M.N. Use of a Green Channel in Remote Sensing of Global Vegetation from EOS-MODIS. *Remote Sens. Environ.* **1996**, *58*, 289–298. [CrossRef]
79. Buschmann, C.; Nagel, E. Variation of Reflectance Signatures of a Leaf as Indication of Physiological Activity. In Proceedings of the IGARSS '93—IEEE International Geoscience and Remote Sensing Symposium, Tokyo, Japan, 18–21 August 1993; Volume 2, pp. 522–524.
80. Gitelson, A.A.; Vina, A.; Arkebauer, T.J.; Rundquist, D.C.; Keydan, G.; Leavitt, B. Remote Estimation of Leaf Area Index and Green Leaf Biomass in Maize Canopies. *Geophys. Res. Lett.* **2003**, *30*, 4–7. [CrossRef]
81. Daughtry, C.S.T.; Walthall, C.L.; Kim, M.S.; de Colstoun, E.B.; McMurtrey, J.E. Estimating Corn Leaf Chlorophyll Concentration from Leaf and Canopy Reflectance. *Remote Sens. Environ.* **2000**, *74*, 229–239. [CrossRef]
82. Pañuelas, J.; Baret, F.; Filela, I. Semi-Empirical Indices to Assess Carotenoids/Chlorophyll a Ratio from Leaf Spectral Reflectance. *Photosynthetica* **1995**, *31*, 221–230.
83. Gitelson, A.A.; Merzlyak, M.N.; Zur, Y.; Stark, R.; Gritz, U. Non-Destructive and Remote Sensing Techniques for Non-Destructive and Remote Sensing Techniques for Estimation of Vegetation Status Estimation of Vegetation Status. *Pap. Nat. Resour.* **2001**.
84. Gitelson, A.A.; Stark, R.; Grits, U.; Rundquist, D.; Kaufman, Y.; Derry, D. Vegetation and Soil Lines in Visible Spectral Space: A Concept and Technique for Remote Estimation of Vegetation Fraction. *Int. J. Remote Sens.* **2002**, *23*, 2537–2562. [CrossRef]
85. Huete, A.; Didan, K.; Miura, T.; Rodriguez, E.P.; Gao, X.; Ferreira, L.G. Overview of the Radiometric and Biophysical Performance of the MODIS Vegetation Indices. *Remote Sens. Environ.* **2002**, *83*, 195–213. [CrossRef]
86. Sulik, J.J.; Long, D.S. Spectral Considerations for Modeling Yield of Canola. *Remote Sens. Environ.* **2016**, *184*, 161–174. [CrossRef]
87. Hunt, D.A.; Tabor, K.; Hewson, J.H.; Wood, M.A.; Reymondin, L.; Koenig, K.; Schmitt-harsh, M.; Follett, F. Review of Remote Sensing Methods to Map Co Ff Ee Production Systems. *Remote Sens.* **2011**, *12*, 2041. [CrossRef]
88. El-Shikha, D.M.; Barnes, E.M.; Clarke, T.R.; Hunsaker, D.J.; Haberland, J.A.; Pinter, P.J., Jr.; Waller, P.M.; Thompson, T.L. Remote Sensing of Cotton Nitrogen Status Using the Canopy Chlorophyll Content Index (CCCI). *Trans. ASABE* **2008**, *51*, 73–82. [CrossRef]

89. Haboudane, D.; Miller, J.R.; Tremblay, N.; Zarco-Tejada, P.J.; Dextraze, L. Integrated Narrow-Band Vegetation Indices for Prediction of Crop Chlorophyll Content for Application to Precision Agriculture. *Remote Sens. Environ.* **2002**, *81*, 416–426. [CrossRef]
90. Rondeaux, G.; Steven, M.; Baret, F. Optimization of Soil-Adjusted Vegetation Indices. *Remote Sens. Environ.* **1996**, *55*, 95–107. [CrossRef]
91. Andreatta, D.; Gianelle, D.; Scotton, M.; Dalponte, M. Estimating Grassland Vegetation Cover with Remote Sensing: A Comparison between Landsat-8, Sentinel-2 and PlanetScope Imagery. *Ecol. Indic.* **2022**, *141*, 109102. [CrossRef]
92. Roujean, J.L.; Breon, F.M. Estimating PAR Absorbed by Vegetation from Bidirectional Reflectance Measurements. *Remote Sens. Environ.* **1995**, *51*, 375–384. [CrossRef]
93. Jordan, C.F. Derivation of Leaf-Area Index from Quality of Light on the Forest Floor. *Ecology* **1969**, *50*, 663–666. [CrossRef]
94. Wu, W. The Generalized Difference Vegetation Index (GDVI) for Dryland Characterization. *Remote Sens.* **2014**, *6*, 1211–1233. [CrossRef]
95. Richardson, A.J.; Everitt, J.H. Using Spectral Vegetation Indices to Estimate Rangeland Productivity. *Geocarto Int.* **1992**, *7*, 63–69. [CrossRef]

Disclaimer/Publisher's Note: The statements, opinions and data contained in all publications are solely those of the individual author(s) and contributor(s) and not of MDPI and/or the editor(s). MDPI and/or the editor(s) disclaim responsibility for any injury to people or property resulting from any ideas, methods, instructions or products referred to in the content.